Hydrogels

International Edition: DOI: 10.1002/anie.201907880
German Edition: DOI: 10.1002/ange.201907880

# Design Parameters of Tissue-Engineering Scaffolds at the Atomic Scale

*Shehrazade Jekhmane, Marek Prachar, Raffaele Pugliese, Federico Fontana, João Medeiros-Silva, Fabrizio Gelain,* and Markus Weingarth**

***Abstract:*** *Stem-cell behavior is regulated by the material properties of the surrounding extracellular matrix, which has important implications for the design of tissue-engineering scaffolds. However, our understanding of the material properties of stem-cell scaffolds is limited to nanoscopic-to-macroscopic length scales. Herein, a solid-state NMR approach is presented that provides atomic-scale information on complex stem-cell substrates at near physiological conditions and at natural isotope abundance. Using self-assembled peptidic scaffolds designed for nervous-tissue regeneration, we show at atomic scale how scaffold-assembly degree, mechanics, and homogeneity correlate with favorable stem cell behavior. Integration of solid-state NMR data with molecular dynamics simulations reveals a highly ordered fibrillar structure as the most favorable stem-cell scaffold. This could improve the design of tissue-engineering scaffolds and other self-assembled biomaterials.*

## Introduction

Stem cells respond to their microenvironment, which provides critical cues for their migration, differentiation, and proliferation.[1–5] The regulatory interplay between stem cells and their native extracellular matrix has important implications for the design of biomimetic tissue-engineering scaffolds, with potentially exciting applications in regenerative medicine that could lead to a paradigm shift in therapeutic treatments.[6–10] In order to improve our capabilities in engineering tissues, in-depth understanding of properties of stem cell substrates is essential.[2,4,10–12] Furthermore, it has been recognized by cell biologists that a better understanding of designer matrices is critical for progress in translational research with stem cells and organoids.[13]

Commonly, nano- or macroscale biophysical tools are used for the characterisation of biomimetic stem-cell substrates.[3] Information at the atomic scale is very scarce, although such information could critically improve the design of stem-cell substrates, and enable to distinguish materials that exhibit similar properties on higher length scales.[5] Indeed, atomic-scale information could enable the development of stem-cell substrates with optimized biomechanical parameters,[14,15] improved exposure of functional motifs,[16] better cross-linking strategies,[10,17] tuned nanotopography,[18] or the inclusion of stimuli-responsive elements.[19]

In this work, we discover novel design parameters for neural-tissue scaffolds using solid-state nuclear magnetic resonance (ssNMR), a technique that enables the characterization of soft matter at atomic-level and at close-to physiological conditions. We studied a series of peptidic hydrogels that were designed to self-assemble into biocompatible scaffolds for the treatment of spinal-cord injury (SCI),[20] a damage for which no medical cure is available, yet a growing body of evidence suggests that biomechanical cues can guide SCI repair.[21,22] The peptides display variants of the bone marrow homing peptide 1 (BMHP1) functional motif that stimulates interactions with neural stem cells, and some peptides feature an N-terminal biotin tag to foster self-assembly (Table 1). The most favorable hydrogels showed attractive self-healing properties, stimulated human neural stem cell (hNSC) viability and differentiation in vitro, and showed regenerative potential in vivo in a rodent model of SCI.[20]

Here, using an NMR approach that works at natural isotope abundance and enables the fast screening of complex materials, we present decisive molecular determinants, such as the homogeneity and the self-assembly degree of the scaffold, that directly correlate with hNSC viability. Moreover, using an advanced ssNMR setup that works with as little as 60 nmol of unlabelled material, we succeed to understand how supramolecular structures of stem-cell substrates relate to favorable functional properties, which we correlate to macroscopic atomic force microscopy (AFM) and rheology data. Altogether, our study presents ssNMR as a broadly applicable, high-resolution technique to gauge tissue-engineering scaffolds that, in combination with other methods,

[*] S. Jekhmane, M. Prachar, J. Medeiros-Silva, Dr. M. Weingarth
NMR Spectroscopy, Bijvoet Center for Biomolecular Research, Department of Chemistry, Faculty of Science, Utrecht University
Padualaan 8, 3584 CH Utrecht (The Netherlands)
E-mail: m.h.weingarth@uu.nl
R. Pugliese, F. Fontana, Dr. F. Gelain
Fondazione IRCCS Casa Sollievo della Sofferenza, Unita' di Ingegneria Tissutale
Viale Cappuccini 1, 71013 San Giovanni Rotondo (Italy)
E-mail: f.gelain@css-mendel.it
F. Fontana, Dr. F. Gelain
ASST Grande Ospedale Metropolitano Niguarda, Center for Nanomedicine and Tissue Engineering
Piazza dell'Ospedale Maggiore 3, 20162 Milan (Italy)

Supporting information, including details of the NMR, AFM, and rheological measurements, functional assays, sample preparation, solution NMR spectra, and the assembly pathway from MD simulations, and the ORCID identification number(s) for the author(s) of this article can be found under: https://doi.org/10.1002/anie.201907880.

*Table 1:* List of BMHP1-derived peptides and ssNMR analysis of the hydrogel-mechanics. The hydrogel classification is based on the signal intensities in Figure 1. Rigid hydrogels give intense dipolar and faint scalar signals, respectively, while mobile hydrogels give faint dipolar and intense scalar signals. Hydrogels 2 and B26 were classified as highly mobile because they showed by far the strongest scalar and no or vanishingly small dipolar signals.

| Name | Peptide Sequence | ssNMR analysis (hydrogel) |
|---|---|---|
| 2 | Acetyl-GGGPFSSTKT-CONH2 | highly mobile |
| B3 | Biotin-GGGPFSSTKT-CONH2 | rigid |
| 4 | Acetyl-WGGGPFSSTKT-CONH2 | mobile |
| B15 | Biotin-GGGAFSSTKT-CONH2 | rigid |
| B24 | Biotin-GGGAFASTKT-CONH2 | rigid |
| B26 | Biotin-GGGPFASTKT-CONH2 | highly mobile |
| 30 | Acetyl-WGGGAFASTKT-CONH2 | mobile |
| 31 | Acetyl-WGGGAFSSTKT-CONH2 | mobile |

enables a holistic characterization of stem-cell substrates from the atomic to the macroscopic length scale.

## Results and Discussion

### Mechanical Characterization at the Atomic Scale

We prepared a series of self-organized BMHP1-peptide hydrogels at a concentration of 3% w/v (Table 1). First, we analyzed the mechanical properties of the highly hydrated samples using high-resolution ssNMR. We quantified the rigid and dynamic fractions of the hydrogels using one-dimensional (1D) so-called dipolar NMR experiments (i.e., experiments that rely on the presence of dipolar couplings between $^{1}H$ and $^{13}C$) that detect immobile molecular components, and scalar NMR experiments that report on mobile components with pronounced fast pico-to-nanosecond dynamics that do not form stable, large assemblies (Figure 1 A,B). Remarkably, our experiments, which were performed without synthetic $^{13}C$-isotope enrichment, revealed clear mechanical differences between the hydrogels. The hydrogels formed by peptides 2 (dubbed hydrogel 2) and B26 gave intense scalar spectra and virtually no dipolar signal. This implies that peptides in these two hydrogels are highly mobile, weakly associated, and do not form larger aggregates. We confirmed that the scalar spectra of the hydrogels relate to fast tumbling, small assemblies or free peptides by solution NMR measurements of free peptides that yielded exactly the same signals (Supporting Information, Figure S1). In stark contrast, the biotinylated hydrogels B3, B15, and B24 gave intense dipolar spectra and very faint scalar signals, implying high rigidity and high assembly degrees. Intriguingly, the rigid hydrogels B15 and especially B24 performed best in previous cell viability assays[20] in which the BMHP1-derived scaffolds were used as substrates to culture hNSCs, a well-standardized source of somatic human stem cells for in vitro testing of peptidic biomaterials,[23,24] while the mobile hydrogels exhibited no significant difference to the negative control. Thereby, the data strongly suggest that the appropriate mechanical stiffness at the molecular level of the hydrogel is a crucial functional factor.

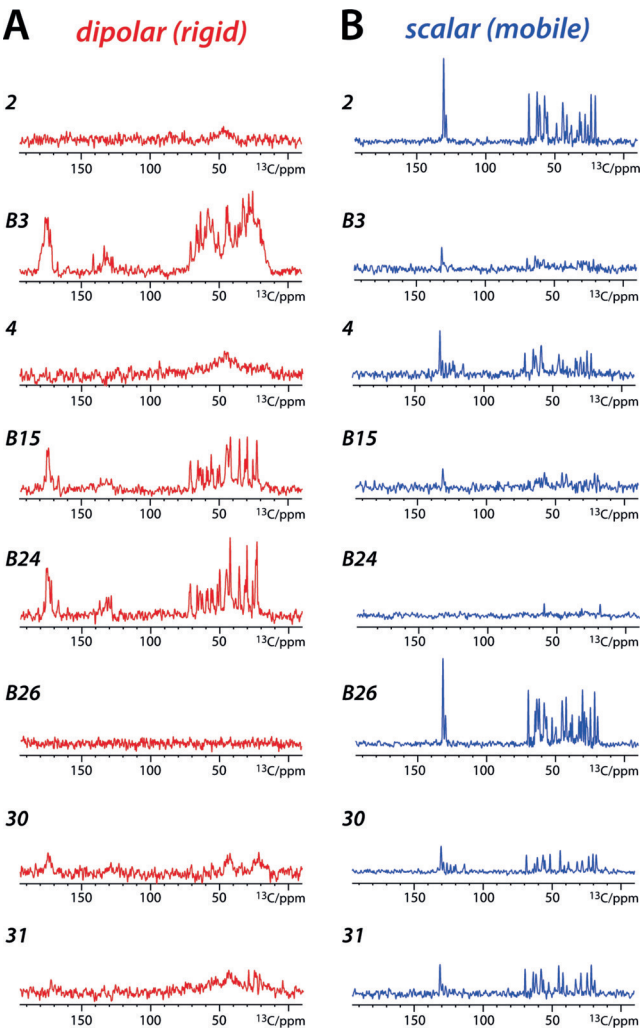


*Figure 1.* The mechanical properties of the hydrogels at the atomic scale. A) $^{13}C$-detected dipolar cross-polarization ssNMR spectra that characterize the immobile fraction of the hydrogels. B) $^{13}C$-detected scalar INEPT ssNMR spectra that characterize dynamic molecular components with fast nanosecond motion and large amplitudes. All spectra were acquired at 500 MHz, 10 kHz magic angle spinning (MAS), and at 280 K sample temperature.

Remarkably, only in hydrogel B24, the best performing stem-cell substrate, virtually all scalar signals completely disappeared. Furthermore, the aromatic Phe5 sidechain in the middle of the peptides, which mutational studies suggest to be a hotspot for peptide assembly, is only completely rigidified in scaffold B24.[25] This implies that all peptides are firmly assembled in hydrogel B24, which strongly suggests that this is favorable for the culturing of hNSCs, and which we investigate in detail below.

### The Structure of the Peptides in the Scaffold

As a next step, we investigated the impact of the peptide conformation in the supramolecular environment on the functional properties. Therefore, we sought to quantitatively assign the NMR chemical shifts, which are delicate reporters

  

of peptide conformation.[26] However, quantitative chemical-shift assignments of solid-like decametric peptides with complex tags require two-dimensional (2D) spectra. Unfortunately, such spectra usually necessitate isotope enrichment, which drastically limits the applicability of NMR because of severely increased material costs and the high complexity of labelling certain materials. Here, we demonstrate extensive proton and carbon assignments of solid-like hydrogels at natural isotope abundance and physiological temperatures using a $^{1}$H-detected ssNMR setup that strongly increases signal sensitivity and requires less than 75 μg (60 nmol) of unlabelled peptide.[27–35] To our knowledge, this is the first time that $^{1}$H-detected ssNMR has been successfully used to quantitatively assign solid-like peptide hydrogels at natural abundance, suggesting that this is a highly promising technique for the quantification of such materials in the future.

We acquired a $^{1}$H-detected dipolar 2D $^{13}$C-$^{1}$H correlation spectrum of scaffold B24 at 800 MHz magnetic field and 60 kHz magic angle spinning (MAS, Figure 2A). We carefully verified that the signal positions were exactly the same at 15 and 60 kHz MAS, demonstrating that the scaffold structure is not modulated by the sample spinning frequency (Supporting Information, Figure S2). The 2D $^{13}$C-$^{1}$H spectrum exhibited a very favorable spectral resolution and we could readily identify most of the signals by their characteristic chemical shifts. Such fingerprint signals were the Gly1–3 CαHα, Phe5 CβHβ, Ser7 CβHβ, and Ala/Thr CαHα and CβHβ. The Ser7 CαHα signal could be unambiguously identified by comparison with hydrogel B15, which has two serine residues and features a much stronger signal at 57 $^{13}$C ppm. We could also assign the biotin tag, which provided detailed insights into its molecular role in the hydrogel. A comparison with solution NMR spectra of free B24 peptides shows significant chemical shift perturbations of more than one ppm for several biotin carbons (C2, C3, C6, and C9, Supporting Information, Figure S3),[36] demonstrating that biotin changes its conformation in the hydrogel. These data imply that biotin is actively involved in the self-assembly procedure and most likely rigidly packed in the hydrophobic core, agreeing with the critical role of biotin for the formation of rigid hydrogels (Figure 1). With these extensive assignments, we were able to determine the conformation of the assembled B24 peptides at high-resolution (Figure 2B,C). This analysis revealed that residues Ala4-Phe5-Ala6-Ser7-Thr8-Lys9 adopt β-strand conformation in hydrogel B24, while residue Thr10 has reduced β-strand propensity. Note that the free peptide B24 adopts a random coil structure (Supporting Information, Figure S4).

### *The Order of the Scaffold as a Novel Design Parameter*

With the help of our detailed structural knowledge of B24, we sought to understand the molecular structure of the other, functionally less favorable hydrogels. Particularly, we hypothesized that further, thus far ignored, material properties exist that critically influence the use of hydrogels as hNSC substrates. Indeed, while an appropriate rigidity (usually between 100 and 1000 Pa at the macroscale) is important for neural-tissue engineering scaffolds,[37] rigidity is clearly not the only decisive factor: while hydrogels B3, B15, and B24 all showed high rigidity in ssNMR spectra, B15/B24 outperformed hydrogel B3 in previously published cell viability assays.[20] We decided to acquire dipolar spectra for a selection of five hydrogels (2, B3, B15, B24, 30) at a very high magnetic field of 950 MHz, which strongly improves NMR spectral quality (Figure 2E). Indeed, at 950 MHz, we succeeded to quantitatively understand the molecular structure of the hydrogels, and we demonstrate that the sample homogeneity and assembly degree are new material properties of striking importance.

At 950 MHz, hydrogels B15 and B24 yield very similar dipolar spectra with many remarkably sharp signals of less than 0.3 $^{13}$C ppm, demonstrating that both scaffolds are highly ordered and adopt extended conformations from residues Ala4 to Thr10. However, while B24 shows virtually no sign of heterogeneity, a number of B15 signals, such as Lys9 and Thr10 in the functional C-terminus, are broadened (Figure 2D). Especially the critical residue Phe5 shows increased heterogeneity for both Cα (0.58 and 0.34 $^{13}$C ppm in B15 and B24, respectively) and Cβ (0.66 and 0.21 $^{13}$C ppm in B15 and B24, respectively). The increased disorder of Phe5 correlates with residual scalar signal of Phe5 in B15 and the reduced assembly degree of B15 (Figure 1), while all peptides are assembled in the extraordinarily homogeneous scaffold B24. Surprisingly, our 950 MHz data reveal that scaffold B3 is a polymorph (Figure 2E) that consists of i) a dominant ordered conformation with sharp signals (0.3–0.4 $^{13}$C ppm) and ii) a multitude of unstructured peptides that give very broad signals. The polymorphism of B3 is readily visible by the broad signal feed and the signals in the spectral region below 20 $^{13}$C ppm that corresponds to unstructured peptides and is empty in B15/B24. Most likely, the heterogeneity of B3 results from the Pro residue in the middle of the peptide, which impedes the formation of ordered supramolecular structures, and which is replaced by an Ala in B15 and B24. The observed sample heterogeneity can either relate to static molecular disorder and/or slowly exchanging conformations. Notably, the functional C-terminal BMHP1 motif that fosters stem-cell contacts changes from β-strand to coil conformation in hydrogel B3, as we can unambiguously determine from the lower chemical shifts of Thr8β/Thr10β (70.9/70.4 and 72.1/71.4 $^{13}$C ppm in B3 and B24, respectively) and the much higher shifts of Lys9Cα (54.8 and 51.7 $^{13}$C ppm in B3 and B24, respectively). Most importantly, the reduced secondary structure and decreased order that we observe in scaffold B3 and other stem-cell scaffolds (see below) correlate with less favorable functional properties, as demonstrated in previous cell viability assays.[20] Future atomic-scale studies with other designer stem-cell scaffolds would be highly insightful to gauge and generalize our findings.[13]

We also acquired dipolar spectra at 950 MHz for the mobile hydrogel 30 and the highly mobile hydrogel 2 in order to understand the molecular properties of the small rigid fractions of these scaffolds with low assembly degrees (Figure 2E). Since the rigid fractions are the minor fractions in mobile and very mobile hydrogels, we required drastically longer measurement times (180000 signal accumulations/sample, i.e., 5 days for each sample) in order to obtain clear

  

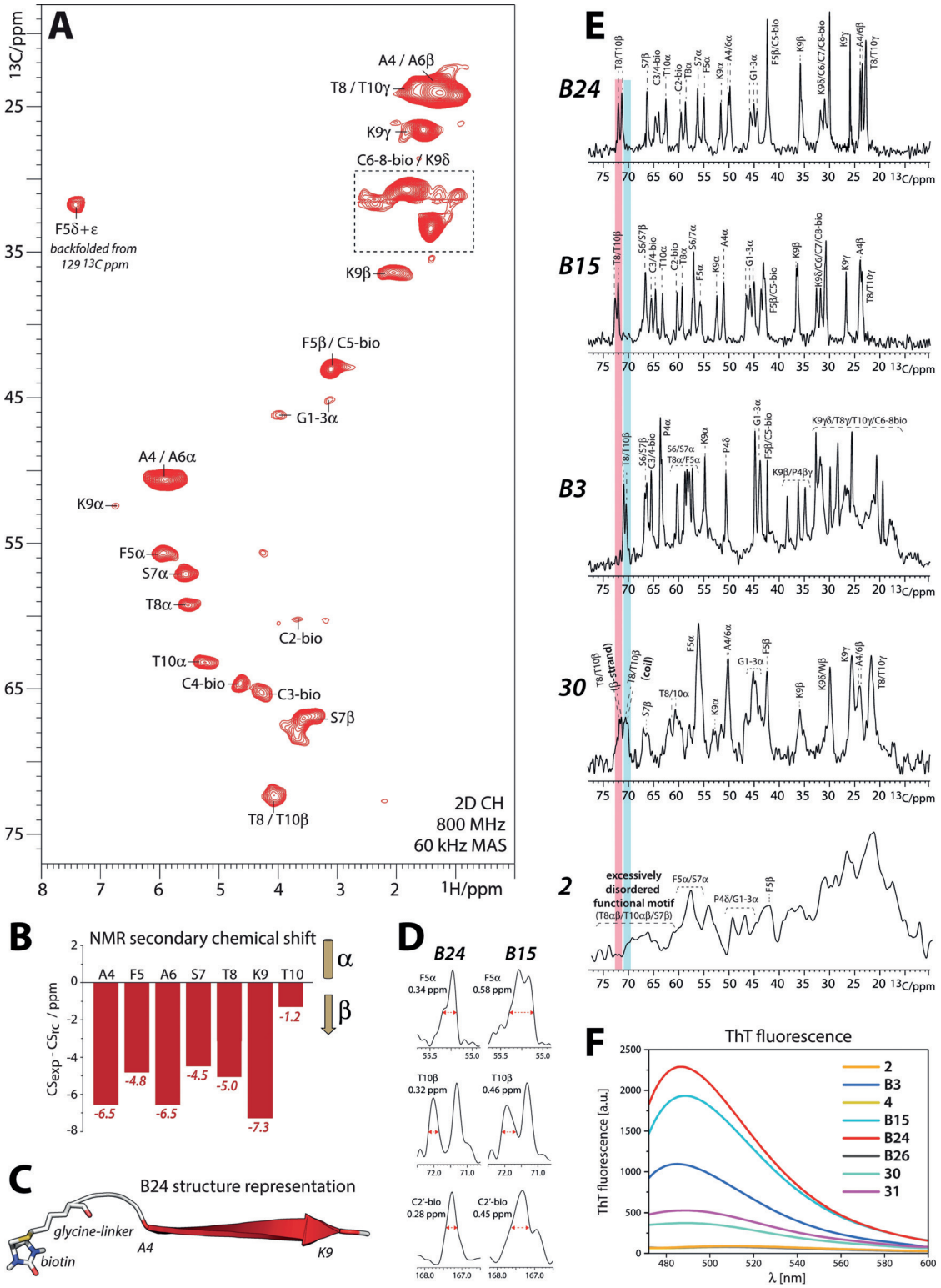


***Figure 2.*** The conformation and dispersity of the assembled peptides at high resolution. A) $^{1}$H-detected 2D $^{13}$C-$^{1}$H spectrum of hydrogel B24 at natural abundance, acquired at 800 MHz using 60 kHz MAS and 305 K sample temperature. B) [Cα-Cβ] secondary chemical shift (SCS)[26] analysis reveals pronounced β-strand conformation for residues Ala4-Thr10. C) Structural representation of the assembled peptide B24 derived from ssNMR. D) Cross-sections of $^{13}$C dipolar signals of B24 (left panel) and B15 (right). The linewidth at half-height is indicated. E) ssNMR spectra of hydrogels 2, B3, B15, B24, and 30 acquired at 950 MHz using 15 kHz MAS. 30000 signals were accumulated for the rigid hydrogels (B3, B15, B24), and 180000 accumulations for the mobile hydrogel 30 and the very mobile hydrogel 2. Spectra were processed with exponential line-broadening (10 Hz for hydrogels B3, B15, and B24; 30 Hz for hydrogel 30; 200 Hz for hydrogel 2). The red and blue bars mark threonine residues in extended and coiled structures, respectively. F) ThT fluorescence measurements of the hydrogels.

  

dipolar signals. Signals of hydrogel 30 were generally much broader than for B24, which relates to a markedly increased heterogeneity of the assembly. Intriguingly, as can be unambiguously deduced from the doubling of Thr8β/Thr10β signals and the characteristic chemical shifts,[26] hydrogel 30 exhibits both coiled and extended conformations for the functionally critical C-terminus. The substantial disorder of the C-terminus is also readily visible from the Ser7β signal, which is more than four times wider in hydrogel 30 than in B24 (1.43 and 0.34 $^{13}$C ppm in hydrogels 30 and B24, respectively). This situation is even more pronounced for the highly mobile hydrogel 2. While the assembly domain in hydrogel 2 around Phe5 features starkly broadened yet still discernible signals, the functional C-terminus (residues Ser7, Thr8, and Thr10) is extremely disordered and almost broadened beyond detection. Thereby, our quantitative ssNMR analysis demonstrates that the peptide heterogeneity correlates with lower assembly degree, i.e., with more intense scalar signals (Figure 3). This conclusion is confirmed by thioflavin T (ThT) fluorescence measurements that very clearly show that increasing homogeneity/order of the ssNMR spectra goes hand in hand with an increase in ThT fluorescence, i.e., with an increase in stable β-structured assemblies (Figure 2F). Most importantly, a comparison with previous cell viability assays clearly shows that peptide order directly correlates with favorable functional properties.[20] Altogether, these findings demonstrate that the conformational homogeneity and the assembly degree are novel, vital functional factors for peptidic tissue-engineering scaffolds. Interestingly, the recently reported fibers assembled from the gel-forming MAX1 peptide also show an intriguing homogeneity with a single molecular conformation,[38] and these assemblies also exhibit remarkable mechanical bulk stability.[39]

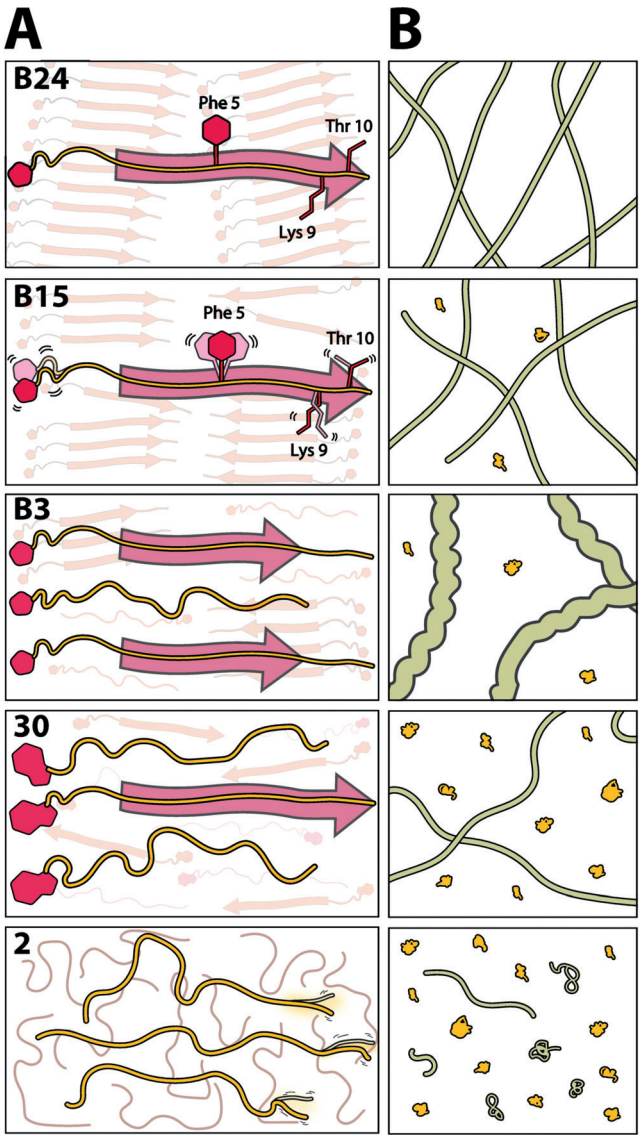


***Figure 3.*** Structuring and assembly from ssNMR. A) Illustration of the building blocks that form fibers and large assemblies. This is based on the dipolar ssNMR data reported in this study. B) The assembly degree of the hydrogels, derived from comparative dipolar and scalar ssNMR data. Strings illustrate fibers that give dipolar NMR signals, while the yellow shapes relate to small assemblies that give scalar signals. The relative thickness of the fibers was derived from AFM data (see below).

### *The Supramolecular Organization of the Scaffolds*

To gain insights into the global arrangement and self-assembly pathway of the hydrogels, we used long and large-scale restrained atomistic molecular dynamics (MD) simulations.[40,41] Initially, we focused on the functionally most favorable hydrogel B24. In order to steer the assembly behavior, we integrated the ssNMR secondary structure information into the MD simulation via TALOS+,[42] a widely used software that derives torsional angles from chemical shifts. We simulated the self-organization of one hundred B24 peptides that were initially randomly distributed in a water-filled box. The peptides rapidly formed smaller clusters within 50 ns. Interestingly, due to the preference for β-strand conformation and their amphiphilic nature, the peptides mostly assemble to extended formations (Supporting Information, Figure S5). These stretched clusters then unite to an elongated fiber-like construct reminiscent of the flat B24 fibers previously observed by AFM.[20] The resulting fibrous assembly spans through the entire simulation box and exhibits a high β-strand content (Figure 4A), in line with ssNMR data.

Next, we analyzed the fiber organization. A molecular contact map (Figure 4E) shows that biotin and Phe5 are the two major intermolecular hotspots. These data demonstrate that the aromatic rings engage in intense π–π-stacking, and that Phe5 and biotin are mutually packed into the core of scaffold B24, which agrees well with our ssNMR results (Figures 1 and 2), and matches with X-ray powder diffraction data.[25] Intriguingly, the functional C-terminus is substantially less involved in peptide–peptide interactions, and hence available to engage in contacts with cellular receptors. Indeed, a calculation of the water exposure shows that hydrophobic N-terminus is buried in the fiber core, while the C-terminal BMHP1 motif forms the functional surface (Figure 4C).

To understand the role of biotin, we replaced biotin by an acetyl tag and performed another simulation of similar size and duration. Furthermore, we did a similar simulation for

  

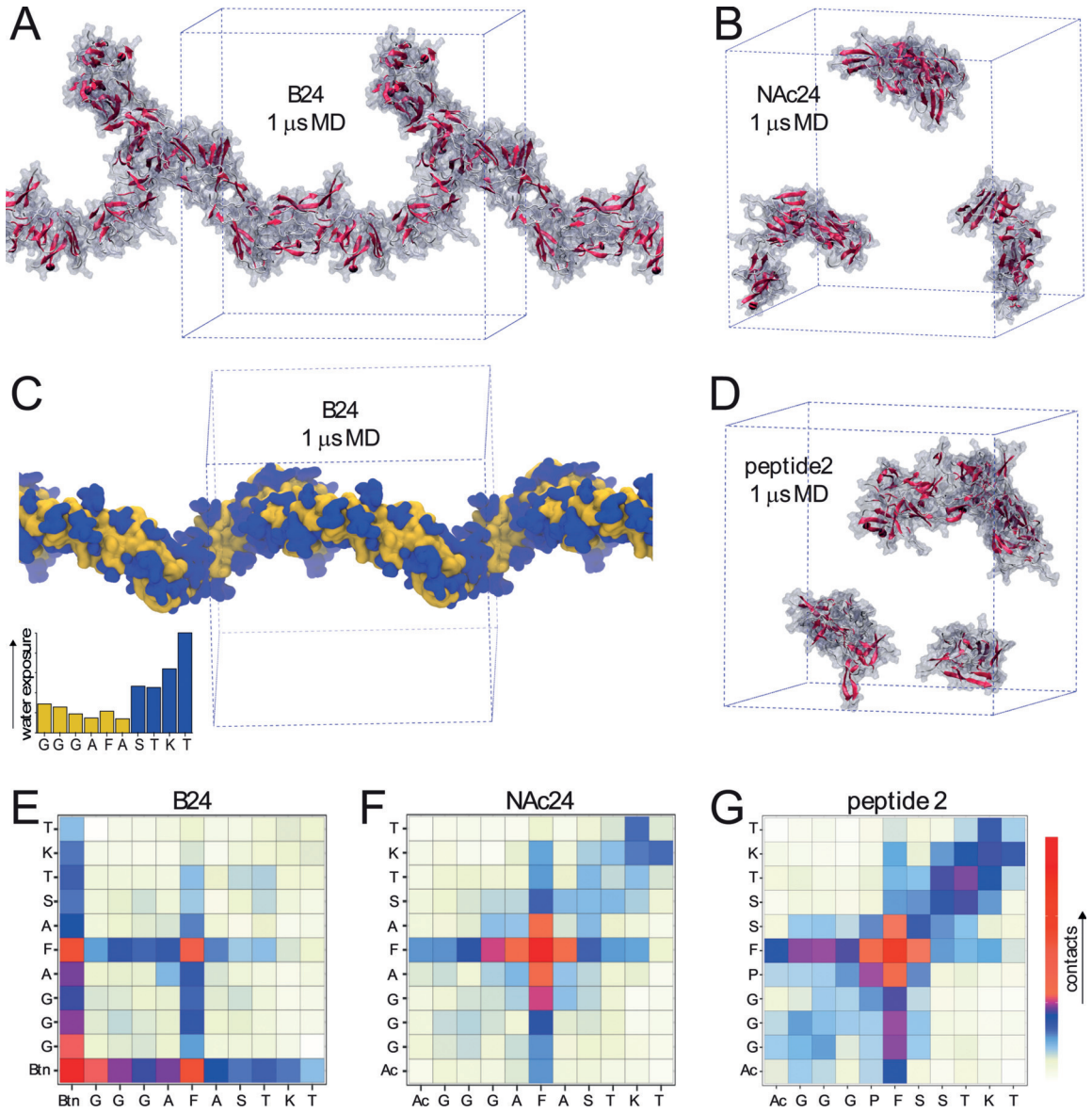


***Figure 4.*** The supramolecular organization. A) B24 fiber-like assembly after 1 µs of restrained atomistic MD simulation. B) Replacing the biotin tag by an acetyl tag markedly reduces the self-organization tendency. C) The functional C-terminus (Ser7-Thr8-Lys9-Thr10, shown in blue) is surface-accessible in the B24 fiber assembly. The N-terminal residues Gly1-Phe6 and biotin are colored in yellow. The insert shows the water exposure derived from the MD simulation. D) Peptide 2 also shows reduced self-organization tendency. E) Residual contact matrix derived from the B24 simulation using a 5 Å cut-off distance. F) Same as (E), but for the N-acetylated peptide 24. G) Same as (E), but for peptide 2.

peptide 2. Interestingly, the acetylated peptides also aggregated to smaller cluster that, however, did not stably combine to longer fiber-like constructs (Figure 4B,D). This observation strongly suggests that biotin critically stimulates the transition from a small stretched cluster to elongated fibers, which agrees well with our ssNMR data and explains why we see substantially weaker dipolar signals for peptide 2 and all peptides without a biotin tag. Remarkably, in the peptides 2 and NAc24, which are not tagged with biotin, the functional C-terminus is much more strongly involved in packing interactions, which is presumably detrimental for its availability as focal point for cellular contacts (Figure 4F,G). In particular, for peptide 2, the C-terminus shows a wide range of intermolecular interactions, explaining the strong broadening of the peptide 2 C-terminus in NMR spectra (Figure 2E). Remarkably, residue Pro4 in peptide 2 increases the disorder, which matches with the polymorphism in hydrogel B3 that features a Pro at the same position (Figure 2E).

### *Comparison to Morphological and Rheological Properties*

Finally, we sought to relate our atomistic insights to morphological and viscoelastic properties. Morphological hydrogel properties are typically studied with AFM. AFM data show that the highly ordered hydrogels B15 and B24 indeed exhibit a markedly different morphology compared to the heterogenous or mobile hydrogels (Figure 5A and

  

Supporting Information, Figure S6). While peptides B15 and B24 assemble into flat tabular fibers, B3 and the other peptides formed twisted fibers/protofibrils or more complex structures, which agrees with previous studies.[20] Interestingly, the height of 1.7–2.1 nm that we measured with AFM for the B24 fibers (Figure 5B) matches well to the height of the simulated B24 fiber-like assembly, which corroborates that our MD simulation is representative for the fiber formation. The AFM data also showed that, compared to peptide B3, B15 and B24 self-organize into a more homogeneous network of nano-fibers. Such a dense three-dimensional fiber-network better resembles the typical features of the native proteins of the extracellular matrix,[43] and this may be one of the reasons why hydrogels B15 and B24 are more suitable as proregenerative substrates. In agreement with ssNMR data, hydrogel 2 only formed sparse nano-dots but no fibers, while hydrogel 30 showed a much lower fiber density (Supporting Information, Figure S6). Intriguingly, B15 and B24 give basically the same AFM morphologies at the nano-scale, while atomic scale ssNMR data show critical differences.

Rheological measurements of the storage (G′) and loss (G″) moduli are commonly used to characterize viscoelastic and mechanical properties of hydrogels. Here, G′ reflects the stiffness, while G″ represents the energy dissipated during the oscillatory test and correlates with the liquid-like response of the hydrogel. The ratio between G′ and G″ provides insights into the viscoelastic profile, i.e., whether a material behaves as an elastic solid ($G' > G''$) or a viscous liquid ($G' < G''$).[44] The assemblies of peptides B3, B15, and B24 showed typical hydrogel-like profiles, featuring a predominantly elastic solid-like behavior (G′) relative to the viscous component (G″) (Figure 5C, left panel), matching with our previous studies.[20] In contrast, the assemblies formed by peptides 2, 4, B26, 30, and 31 showed substantially lower G′ values, implying softer hydrogels and a weaker tendency to assemble (Supporting Information, Figure S7). These data agree very well with our quantitative ssNMR analysis.

We were particularly interested to compare the three rigid hydrogels in order to explore if the polymorphism of scaffold B3 is reflected in rheological properties. In comparison to B3 (G′ value of 1526 Pa), hydrogels B15 and B24 showed more pronounced solid-like properties with an elastic shear modulus G′ of 3606 Pa and 7131 Pa, respectively. Next, we performed strain-to-failure tests in order to assess the hydrogels failure when subjected to a linear strain progression (Figure 5C, right panel). In line with its lower G′ value, B3 showed a strain-to-failure value of 9.8% (corresponding to a stress-to-failure of 13.24 Pa), while hydrogels B15 and B24 exhibited markedly less deformation before failure (1.5% and 2.3%, respectively) together with higher stress-to-failure values (89.07 Pa and 228.3 Pa, respectively). Notably, these results suggest that the higher stability of hydrogels B15/B24 relates to their much higher molecular order observed with ssNMR. Here, the higher bulk mechanical stability of hydrogels B15/B24 likely relates to an optimal molecular packing, maximizing interresidual and intermolecular contacts,[39]

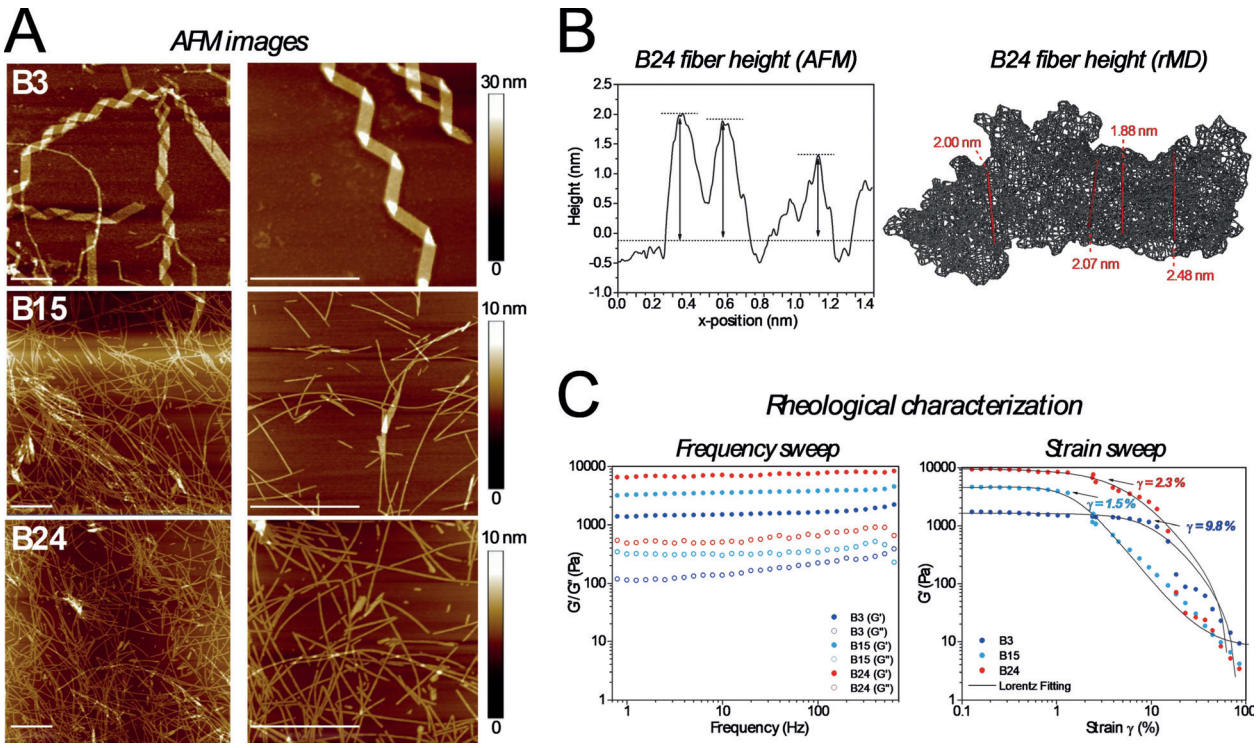


***Figure 5.*** Morphological and rheological characterization. A) AFM analysis. Peptide B3 assembles into shorter twisted protofibrils, while peptides B15 and B24 form long tabular fibers (scale bar 1 μm). B) (left panel) AFM height measurement of scaffold B24 ranging from 1.7 nm to 2.1 nm. (right panel) We observed similar heights the B24 fiber in restraint MD (rMD) simulation. C) (left panel) Rheological characterization of solutions of assembled peptides B3, B15, and B24 were monitored by frequency sweep tests (0.1–1000 Hz) at low strains (1%). The assemblies showed typical hydrogel-like profiles featuring a predominant elastic solid-like behavior (G′, solid dots), compared with the viscous component (G″, empty dots). (right panel) In strain-to-failure tests, hydrogels B15 and B24 are less prone to deformation than B3.

  

while the packing is compromised in disordered samples, which can be associated with reduced mechanical stability.[45] Altogether, we demonstrate that ssNMR, AFM, and rheology provide highly complementary insights at different length scales into the material and functional properties of tissue-engineering scaffolds.

## Conclusion

Here, we have integrated solid-state NMR and MD simulations to characterize the mechanical, topological, and molecular properties of tissue-engineering scaffolds at the atomic scale. Importantly, thanks to modern $^{1}$H-detected ssNMR methods, this approach works without synthetic isotope enrichment and thereby enables studies at low costs and with hard-to-label materials, such as cross-linkers or chemical modifications. On the example of functionalized hydrogels for the treatment of SCI, we were able to relate material and molecular parameters to the viability of hNSCs. Intriguingly, we established that the complete assembly of all peptides to a highly ordered matrix is highly favorable for hNSC survival. Moreover, we demonstrate that the molecular homogeneity of the scaffold relates to favorable functional properties. The order of the stem-cell scaffold presumably enables an optimal exposure of the functional BMHP1 motif that fosters beneficial interactions with hNSCs,[20] while the exposure of the BMHP1 motif is suboptimal in disordered scaffolds due to a distribution of favorable and unfavorable conformations. In the functionally most beneficial hydrogels, homogeneity is achieved by the removal of prolines from the BMHP1 motif. This is a particularly noteworthy finding, given that collagen, the major fibrillar protein of the natural extracellular matrix, has a high proline content (approximately 10 %)[46] yet has only moderate adhesion and very low differentiation potential for hNSCs in vitro.[47] Interestingly, pioneering solid-state NMR studies of bone collagen and cartilage[46,48–56] show that prolines are involved in expansion joints that confer flexibility to collagen fibers,[57] which is vital for the functional mechanics of these native tissues. This finding would suggest that different cell types require different material properties at the atomic-length scale, opening the door to future investigations of novel biomaterials dedicated for other targeted tissues. Moreover, while it is well known that the mechanical properties of stem-cell scaffolds correlate with the functional performance of biological and designer matrices,[5] we show here that the rigidity at the molecular level also correlates with function. This is an important finding given that macroscopic characterizations of material properties only provide an average over atomistic, nanoscopic, and microscopic scales. We also like to underscore that previous microscopic biophysical characterizations did not succeed in quantifying the molecular differences of the stem-cell scaffolds discussed in this study.[20] The latter clearly speaks in favor of ssNMR as a powerful additional tool to understand the properties of designer matrices under physiological conditions. Thereby, the integration of microscopic and macroscopic data with atomistic ssNMR data promises a markedly enhanced and holistic understanding of the material properties of designer stem-cell matrices.

In this regard, the future challenge is to characterize tissue-engineering scaffolds in the presence of stem cells at the atomic-length scale. Here, ssNMR, in combination with advanced detection, enhancement, and sample preparation schemes for complex cellular samples such as dynamics nuclear polarization,[52,58,60] ultrafast MAS,[28] and $^{19}$F-labelling[61,62] could be an ideal tool to enhance our knowledge on interactions between stem cells and their substrates at physiological conditions, and to generally improve our understanding of the composition of bone and tissue materials.

## Acknowledgements

This work was funded by the Netherlands Science Organisation for Scientific Research (NWO, grant numbers 723.014.003 and 711.018.001 to MW) and by the "Ricerca Corrente" fund granted by the Italian Ministry of Health. Experiments at the 950 MHz instrument were supported by uNMR-NL, an NWO-funded Roadmap NMR Facility (no. 184.032.207).

## Conflict of interest

The authors declare no conflict of interest.

**Keywords:** hydrogels · regenerative medicine · self-assembling peptides · solid-state NMR · tissue engineering

**How to cite:** *Angew. Chem. Int. Ed.* **2019**, *58*, 16943 – 16951
*Angew. Chem.* **2019**, *131*, 17099 – 17107

[1] D. T. Scadden, *Nature* **2006**, *441*, 1075 – 1079.
[2] K. H. Vining, D. J. Mooney, *Nat. Rev. Mol. Cell Biol.* **2017**, *18*, 728 – 742.
[3] L. R. Smith, S. Cho, D. E. Discher, *Physiology* **2018**, *33*, 16 – 25.
[4] J. W. Shin, D. J. Mooney, *Cell Stem Cell* **2016**, *18*, 16 – 19.
[5] F. Guilak, D. M. Cohen, B. T. Estes, J. M. Gimble, W. Liedtke, C. S. Chen, *Cell Stem Cell* **2009**, *5*, 17 – 26.
[6] F. J. O'Brien, *Mater. Today* **2011**, *14*, 88 – 95.
[7] A. S. Mao, D. J. Mooney, *Proc. Natl. Acad. Sci. USA* **2015**, *112*, 14452 – 14459.
[8] G. S. Hussey, J. L. Dziki, S. F. Badylak, *Nat. Rev. Mater.* **2018**, *3*, 159 – 173.
[9] L. Yang, S. D. Chueng, Y. Li, M. Patel, C. Rathnam, G. Dey, L. Wang, L. Cai, K. B. Lee, *Nat. Commun.* **2018**, *9*, 3147.
[10] F. Brandl, F. Sommer, A. Goepferich, *Biomaterials* **2007**, *28*, 134 – 146.
[11] E. Gazit, *Chem. Soc. Rev.* **2007**, *36*, 1263 – 1269.
[12] L. Adler-Abramovich, E. Gazit, *Chem. Soc. Rev.* **2014**, *43*, 6881 – 6893.
[13] N. Gjorevski, N. Sachs, A. Manfrin, S. Giger, M. E. Bragina, P. Ordonez-Moran, H. Clevers, M. P. Lutolf, *Nature* **2016**, *539*, 560 – 564.
[14] M. Halperin-Sternfeld, M. Ghosh, R. Sevostianov, I. Grigoriants, L. Adler-Abramovich, *Chem. Commun.* **2017**, *53*, 9586 – 9589.
[15] P. Stock, J. J. Monroe, T. Utzig, D. J. Smith, M. S. Shell, M. Valtiner, *ACS Nano* **2017**, *11*, 2586 – 2597.

  

[16] K. Alberti, R. E. Davey, K. Onishi, S. George, K. Salchert, F. P. Seib, M. Bornhauser, T. Pompe, A. Nagy, C. Werner, P. W. Zandstra, *Nat. Methods* **2008**, *5*, 645 – 650.
[17] J. Zhu, R. E. Marchant, *Expert Rev. Med. Devices* **2011**, *8*, 607 – 626.
[18] C. J. Bettinger, Z. T. Zhang, S. Gerecht, J. T. Borenstein, R. Langer, *Adv. Mater.* **2008**, *20*, 99 – 103.
[19] D. J. Smith, G. A. Brat, S. H. Medina, D. D. Tong, Y. Huang, J. Grahammer, G. J. Furtmuller, B. C. Oh, K. J. Nagy-Smith, P. Walczak, G. Brandacher, J. P. Schneider, *Nat. Nanotechnol.* **2016**, *11*, 95 – 102.
[20] F. Gelain, D. Silva, A. Caprini, F. Taraballi, A. Natalello, O. Villa, K. T. Nam, R. N. Zuckermann, S. M. Doglia, A. Vescovi, *ACS Nano* **2011**, *5*, 1845 – 1859.
[21] K. Franze, P. A. Janmey, J. Guck, *Annu. Rev. Biomed. Eng.* **2013**, *15*, 227 – 251.
[22] R. Schlüßler, S. Mollmert, S. Abuhattum, G. Cojoc, P. Muller, K. Kim, C. Mockel, C. Zimmermann, J. Czarske, J. Guck, *Biophys. J.* **2018**, *115*, 911 – 923.
[23] F. Gelain, A. Horii, S. Zhang, *Macromol. Biosci.* **2007**, *7*, 544 – 551.
[24] F. Gelain, D. Bottai, A. Vescovi, S. Zhang, *PloS one* **2006**, *1*, e119.
[25] D. Silva, A. Natalello, B. Sanii, R. Vasita, G. Saracino, R. N. Zuckermann, S. M. Doglia, F. Gelain, *Nanoscale* **2013**, *5*, 704 – 718.
[26] Y. Wang, O. Jardetzky, *Protein Sci.* **2002**, *11*, 852 – 861.
[27] V. Chevelkov, K. Rehbein, A. Diehl, B. Reif, *Angew. Chem. Int. Ed.* **2006**, *45*, 3878 – 3881; *Angew. Chem.* **2006**, *118*, 3963 – 3966.
[28] K. H. Mroue, Y. Nishiyama, M. K. Pandey, B. Gong, E. McNerny, D. H. Kohn, M. D. Morris, A. Ramamoorthy, *Sci. Rep.* **2015**, *5*, 11991.
[29] J. Stanek, L. B. Andreas, K. Jaudzems, D. Cala, D. Lalli, A. Bertarello, T. Schubeis, I. Akopjana, S. Kotelovica, K. Tars, A. Pica, S. Leone, D. Picone, Z. Q. Xu, N. E. Dixon, D. Martinez, M. Berbon, N. El Mammeri, A. Noubhani, S. Saupe, B. Habenstein, A. Loquet, G. Pintacuda, *Angew. Chem. Int. Ed.* **2016**, *55*, 15504 – 15509; *Angew. Chem.* **2016**, *128*, 15730 – 15735.
[30] J. Medeiros-Silva, D. Mance, M. Daniels, S. Jekhmane, K. Houben, M. Baldus, M. Weingarth, *Angew. Chem. Int. Ed.* **2016**, *55*, 13606 – 13610; *Angew. Chem.* **2016**, *128*, 13804 – 13808.
[31] T. Sinnige, M. Daniels, M. Baldus, M. Weingarth, *J. Am. Chem. Soc.* **2014**, *136*, 4452 – 4455.
[32] J. S. Retel, A. J. Nieuwkoop, M. Hiller, V. A. Higman, E. Barbet-Massin, J. Stanek, L. B. Andreas, W. T. Franks, B. J. van Rossum, K. R. Vinothkumar, L. Handel, G. G. de Palma, B. Bardiaux, G. Pintacuda, L. Emsley, W. Kuhlbrandt, H. Oschkinat, *Nat. Commun.* **2017**, *8*, 2073.
[33] S. K. Vasa, P. Rovo, R. Linser, *Acc. Chem. Res.* **2018**, *51*, 1386 – 1395.
[34] J. Tolchard, M. K. Pandey, M. Berbon, A. Noubhani, S. J. Saupe, Y. Nishiyama, B. Habenstein, A. Loquet, *J. Biomol. NMR* **2018**, *70*, 177 – 185.
[35] D. Mance, T. Sinnige, M. Kaplan, S. Narasimhan, M. Daniels, K. Houben, M. Baldus, M. Weingarth, *Angew. Chem. Int. Ed.* **2015**, *54*, 15799 – 15803; *Angew. Chem.* **2015**, *127*, 16025 – 16029.
[36] J. H. Bradbury, R. N. Johnson, *J. Magn. Reson.* **1979**, *35*, 217 – 222.
[37] A. Caprini, D. Silva, I. Zanoni, C. Cunha, C. Volontè, A. Vescovi, F. Gelain, *New Biotechnol.* **2013**, *30*, 552 – 562.
[38] K. Nagy-Smith, E. Moore, J. Schneider, R. Tycko, *Proc. Natl. Acad. Sci. USA* **2015**, *112*, 9816 – 9821.
[39] K. Nagy-Smith, P. J. Beltramo, E. Moore, R. Tycko, E. M. Furst, J. P. Schneider, *ACS Cent. Sci.* **2017**, *3*, 586 – 597.
[40] M. Rad-Malekshahi, K. M. Visscher, J. P. Rodrigues, R. de Vries, W. E. Hennink, M. Baldus, A. M. Bonvin, E. Mastrobattista, M. Weingarth, *J. Am. Chem. Soc.* **2015**, *137*, 7775 – 7784.
[41] P. Frederix, I. Patmanidis, S. J. Marrink, *Chem. Soc. Rev.* **2018**, *47*, 3470 – 3489.
[42] Y. Shen, F. Delaglio, G. Cornilescu, A. J. Bax, *Biomol. NMR* **2009**, *44*, 213 – 223.
[43] H. Geckil, F. Xu, X. H. Zhang, S. Moon, U. Demirci, *Nanomedicine* **2010**, *5*, 469 – 484.
[44] G. A. Saracino, D. Cigognini, D. Silva, A. Caprini, F. Gelain, *Chem. Soc. Rev.* **2013**, *42*, 225 – 262.
[45] G. Lamour, R. Nassar, P. H. W. Chan, G. Bozkurt, J. X. Li, J. M. Bui, C. K. Yip, T. Mayor, H. B. Li, H. Wu, J. A. Gsponer, *Biophys. J.* **2017**, *112*, 584 – 594.
[46] J. Schiller, D. Huster, *Biomatter* **2012**, *2*, 115 – 131.
[47] F. Gelain, A. Lomander, A. L. Vescovi, S. G. Zhang, *J. Nanosci. Nanotechnol.* **2007**, *7*, 424 – 434.
[48] L. W. Jelinski, C. E. Sullivan, D. A. Torchia, *Nature* **1980**, *284*, 531 – 534.
[49] D. Huster, J. Schiller, K. Arnold, *Magn. Reson. Med.* **2002**, *48*, 624 – 632.
[50] D. Huster, *Annu. Rep. NMR Spectrosc.* **2008**, *64*, 127 – 159.
[51] P. Z. Zhu, J. D. Xu, N. Sahar, M. D. Morris, D. H. Kohn, A. Ramamoorthy, *J. Am. Chem. Soc.* **2009**, *131*, 17064 – 17065.
[52] W. Y. Chow, R. Rajan, K. H. Muller, D. G. Reid, J. N. Skepper, W. C. Wong, R. A. Brooks, M. Green, D. Bihan, R. W. Farndale, D. A. Slatter, C. M. Shanahan, M. J. Duer, *Science* **2014**, *344*, 742 – 746.
[53] W. Y. Chow, R. Li, I. Goldberga, D. G. Reid, R. Rajan, J. Clark, H. Oschkinat, M. J. Duer, R. Hayward, C. M. Shanahan, *Chem. Commun.* **2018**, *54*, 12570 – 12573.
[54] I. Goldberga, R. Li, M. J. Duer, *Acc. Chem. Res.* **2018**, *51*, 1621 – 1629.
[55] K. H. Mroue, N. MacKinnon, J. D. Xu, P. Z. Zhu, E. McNerny, D. H. Kohn, M. D. Morris, A. Ramamoorthy, *J. Phys. Chem. B* **2012**, *116*, 11656 – 11661.
[56] J. D. Xu, P. Z. Zhu, M. D. Morris, A. Ramamoorthy, *J. Phys. Chem. B* **2011**, *115*, 9948 – 9954.
[57] W. Y. Chow, C. J. Forman, D. Bihan, A. M. Puszkarska, R. Rajan, D. G. Reid, D. A. Slatter, L. J. Colwell, D. J. Wales, R. W. Farndale, M. J. Duer, *Sci. Rep.* **2018**, *8*, 13809.
[58] M. Kaplan, S. Narasimhan, C. de Heus, D. Mance, S. van Doorn, K. Houben, D. Popov-Celeketic, R. Damman, E. A. Katrukha, P. Jain, W. J. C. Geerts, A. J. R. Heck, G. E. Folkers, L. C. Kapitein, S. Lemeer, P. M. P. V. E. Henegouwen, M. Baldus, *Cell* **2016**, *167*, 1241 – 1251.
[59] J. Medeiros-Silva, S. Jekhmane, A. L. Paioni, K. Gawarecka, M. Baldus, E. Swiezewska, E. Breukink, M. Weingarth, *Nat. Commun.* **2018**, *9*, 3963.
[60] S. Narasimhan, S. Scherpe, A. L. Paioni, J. van der Zwan, G. E. Folkers, H. Ovaa, M. Baldus, *Angew. Chem. Int. Ed.* **2019**, *58*, 12969 – 12973; *Angew. Chem.* **2019**, *131*, 13103 – 13107.
[61] M. Roos, T. Wang, A. A. Shcherbakov, M. Hong, *J. Phys. Chem. B* **2018**, *122*, 2900 – 2911.
[62] M. Wang, M. Lu, M. P. Fritz, C. M. Quinn, I. J. L. Byeon, C. H. Byeon, J. Struppe, W. Maas, A. M. Gronenborn, T. Polenova, *Angew. Chem. Int. Ed.* **2018**, *57*, 16375 – 16379; *Angew. Chem.* **2018**, *130*, 16613 – 16617.

Manuscript received: June 24, 2019
Revised manuscript received: September 3, 2019
Accepted manuscript online: October 1, 2019
Version of record online: October 30, 2019

  